JACS Au
AN OPEN ACCESS JOURNAL OF THE AMERICAN CHEMICAL SOCIETY

pubs.acs.org/jacsau
Article

Temperature-Responsive Supramolecular Chiral Switch Achieved by Macrocyclic Confinement

Xuan Zhao, Shuangqi Song, Hengzhi Zhang, Xuejian Zhang,* and Yu Liu*

Cite This: JACS Au 2026, 6, 621−630
Read Online

ACCESS | Metrics & More | Article Recommendations | Supporting Information

ABSTRACT: A series of tunable morphological nanoaggregates are constructed by hydroxypropyl-β/γ-cyclodextrin (HPβ/γCD) and cucurbit[8]uril (CB[8]), respectively, encapsulating phenylalanine dipeptide-modified pyrene (PFF) based on host−guest complexation, which not only exhibits a topological transformation from helical nanofibers of PFF to supramolecular nanoparticles, nanotubes, and nanosheets but also induces chiral transmission from phenylalanine dipeptide to pyrene moiety achieving temperature-controlled supramolecular chiral switches. Unlike the encapsulation of HPβCD to PFF at a 1:1 stoichiometric ratio, HPγCD with larger cavity can encapsulate two PFFs, achieving enhanced fluorescence behavior with quantum yield increasing from 1.66% to 32.14% and circular dichroism (CD) with a negative Cotton effect peak at 440 nm with an asymmetric factor (g_{abs}) of -1.44×10^{-4}. Compared with HPβ/γCD, CB[8] gives a stronger binding affinity of up to 5.99×10^5 M^{-1} and a significant positive CD peak at 450 nm. Molecular dynamics and density functional theory calculations reveal that HPγCD and CB[8] could effectively disrupt the symmetric aggregates and restrict the conformations of PFF to realize the efficient chiroptical transmission. Moreover, PFF-HPγCD and PFF-CB[8] supramolecular chiral switches exhibit reversible thermal responsiveness (20−75 °C) and positive circularly polarized luminescence, which are successfully applied to chiral logic gate and polarization-dependent encryption.

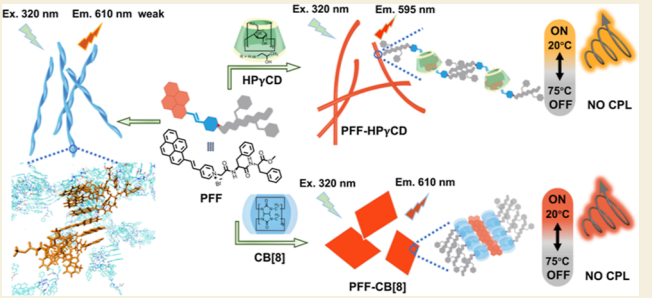

KEYWORDS: *tunable morphologies, supramolecular chiral temperature switches, chiral transmission, macrocyclic confinement, thermal responsiveness*

INTRODUCTION

Chiral supramolecular assemblies based on macrocycles have broad application prospects in fields such as chiral sensing,[1−3] molecular machines,[4−6] chiroptical switches,[7−10] and information encryption[11,12] due to their dynamically adjustable steric configurations and responsiveness to the external stimuli. Supramolecular macrocyclic confinement can modulate the guest's stacking modes and host−guest assembly behaviors often accompanied by changes in topological morphologies,[13−15] thereby expanding fluorescence properties[16−19] and facilitating chirality transfer and amplification.[20−22] Most reported chiral supramolecular assemblies have been achieved by chiral host-induced achiral guests,[23,24] or achiral hosts activated by assembling with chiral guests,[25−27] developing various stimulus-responsive intelligent chiral materials. Cyclodextrins with hydrophobic chiral cavities have been widely reported to significantly induce chiroptical activities through complexation and aggregation with chromophores.[28−30] For example, Stoddart and co-workers demonstrated that γ-cyclodextrin (γCD) formed a 1:2 complex with 1-pyrene carboxylic acid in a cyclodextrin-based metal−organic framework (CD-MOF) exhibiting green fluorescence with a quantum yield (QY) of 38% and obvious circularly polarized luminescence (CPL) with a high asymmetric factor (g_{lum} = $+3.5 \times 10^{-3}$) arising from confinement of a helix-like chiral superstructure within the CD-MOF.[31] Yang et al. designed and synthesized pyrene-substituted γCD to aggregate into nanostrips in aqueous solutions, exhibiting significant circular dichroism (g_{abs} = $+4.3 \times 10^{-2}$) and CPL activities (g_{lum} = $+5.3 \times 10^{-2}$) due to the interpenetration of pyrene units into the γCD cavities.[32] As compared with cyclodextrins, cucurbiturils can specifically recognize and encapsulate positively charged guest molecules with high binding affinities through electrostatic interactions.[33−35] Cao et al. demonstrated that chiral supramolecular organic frameworks were constructed from left-handed (*M*) and right-handed (*P*) rotational chiral tetra(6-coumarinylmethyl-pyridinium) hexaphenylbenzene derivatives and cucurbit[8]uril (CB[8]) in water, which displayed opposite circular dichroism (CD) and CPL spectra

Received: December 3, 2025
Revised: January 6, 2026
Accepted: January 7, 2026
Published: January 13, 2026

Scheme 1. Schematic Illustration of the Assembly Mechanisms and Topological Morphologies of PFF-HPβCD, PFF-HPγCD, and PFF-CB[8] and the Influence of Temperature on the Chiral Supramolecular Assemblies

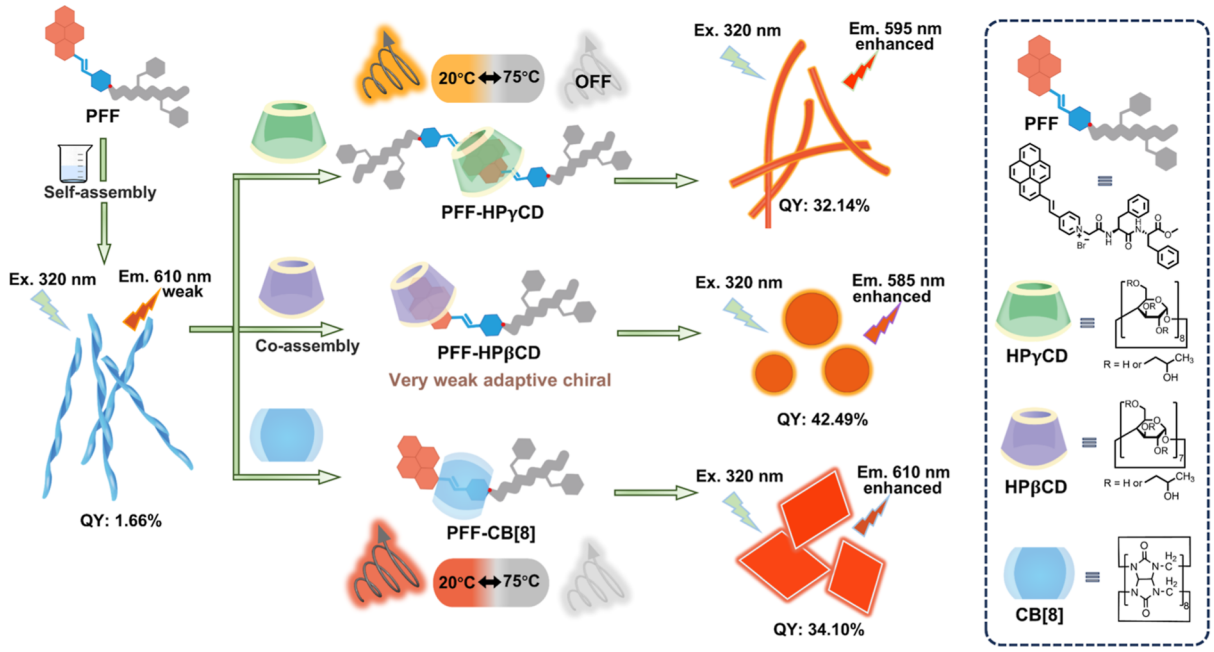

because of the specific recognition properties of CB[8] in the presence of L-PhePhe and L-TrpTrp, respectively.[36]

However, there are few examples of supramolecular chiral switches with reversible temperature responsiveness that activate the chiral transfer of guests through the independent confinement of cyclodextrins and cucurbiturils, accompanied by topological morphology transformation. Herein, we wish to report a novel supramolecular strategy utilizing macrocyclic modulation to achieve tunable morphological and reversible supramolecular chiral temperature switches (Scheme 1). HPβCD, HPγCD, and CB[8] could effectively encapsulate guest-PFF at stoichiometric ratios of 1:1, 1:2, and 1:1, respectively, resulting in the fluorescence enhancement with QYs increasing from 1.66% of phenylalanine dipeptide-modified pyrene (PFF) to 42.49%, 32.14%, and 34.10% through macrocyclic confinement and the topological transformation of PFF from helical nanofibers to supramolecular spherical nanoparticles, fine nanotubes, and rectangular nanosheets. Compared with PFF and PFF-HPβCD, PFF-HPγCD and PFF-CB[8] possessed stronger host−guest interaction with binding affinity up to 1.15×10^6 M^{-2} and 5.99×10^5 M^{-1}, respectively, which could induce obvious chiral transmission by spatial confinement to give strong negative and positive CD signals at 350−600 nm as well as positive CPL emissions. Molecular dynamics (MD) calculations revealed that PFF molecules tend to aggregate via π−π stacking into symmetric aggregates in an aqueous solution, and then, electronic circular dichroism (ECD) calculations of PFF displayed negligible CD signals due to the effective weakening of chiral exciton coupling. Different from PFF nanofibers, density functional theory (DFT) calculations revealed that PFF-HPγCD nanotubes and PFF-CB[8] nanosheets with asymmetric guest alignment and constrained geometries disrupted achiral aggregation and stabilized chiral conformers, leading to pronounced ECD signals. Especially, the chiral PFF-HPγCD and PFF-CB[8] supramolecular switches demonstrated solvent responsiveness and reversible thermal responsiveness within the temperature range of 20−75 °C, achieving dynamically regulated chiral luminescent assembly. This thermally reversible chiral transmission supramolecular strategy was successfully applied to logic gates and polarization-dependent CPL information encryption, providing new insight into well-defined nanostructures and intelligent chiral materials.

RESULTS AND DISCUSSION

PFF was synthesized from 4-(2-(pyren-1-yl)vinyl)pyridine and methyl(2-bromoacetyl)-L-phenylalanyl-L-phenylalaninate via a nucleophilic substitution reaction at the nitrogen of pyridine (Scheme S1) and was characterized by nuclear magnetic resonance (NMR) and high-resolution mass spectrometry (HR-MS) (Figures S1−S3). PFF was designed to contain a pyrene core with a cationic group and a phenylalanine dipeptide moiety (FF) to tune the amphiphilicity in order to facilitate its luminescent behavior and assembly morphology in aqueous solutions. The spectroscopic experiments indicated that the polarity of the solvent significantly influenced the self-assembled luminescence behavior of PFF (Figure S7). The emission intensity at 580 nm in nonpolar dimethyl sulfoxide (DMSO) rapidly decreased and gradually red-shifted to 610 nm as the volume ratio of polar solvent H_2O increased from 0% to 99% accompanied by a decrease in QY from 52.24% to 1.66% (Figures S8 and S9), indicating that PFF has an aggregation-caused quenching (ACQ) characteristic. Moreover, the two-dimensional nuclear Overhauser effect spectroscopy (2D NOESY) spectra of PFF in a solution of different polarities confirmed that the correlation signal of protons on pyrene units significantly increased with the increase in the polarity of the solution (Figure S10), suggesting that the PFF molecules formed tighter π−π stacking aggregates driven by strong hydrophobic interactions.

Subsequently, in order to explore the binding behaviors of HPβ/γCD and CB[8] with PFF, fluorescence and NMR titration experiments were performed. As shown in Figure 1d,

https://doi.org/10.1021/jacsau.5c01631
JACS Au 2026, 6, 621−630

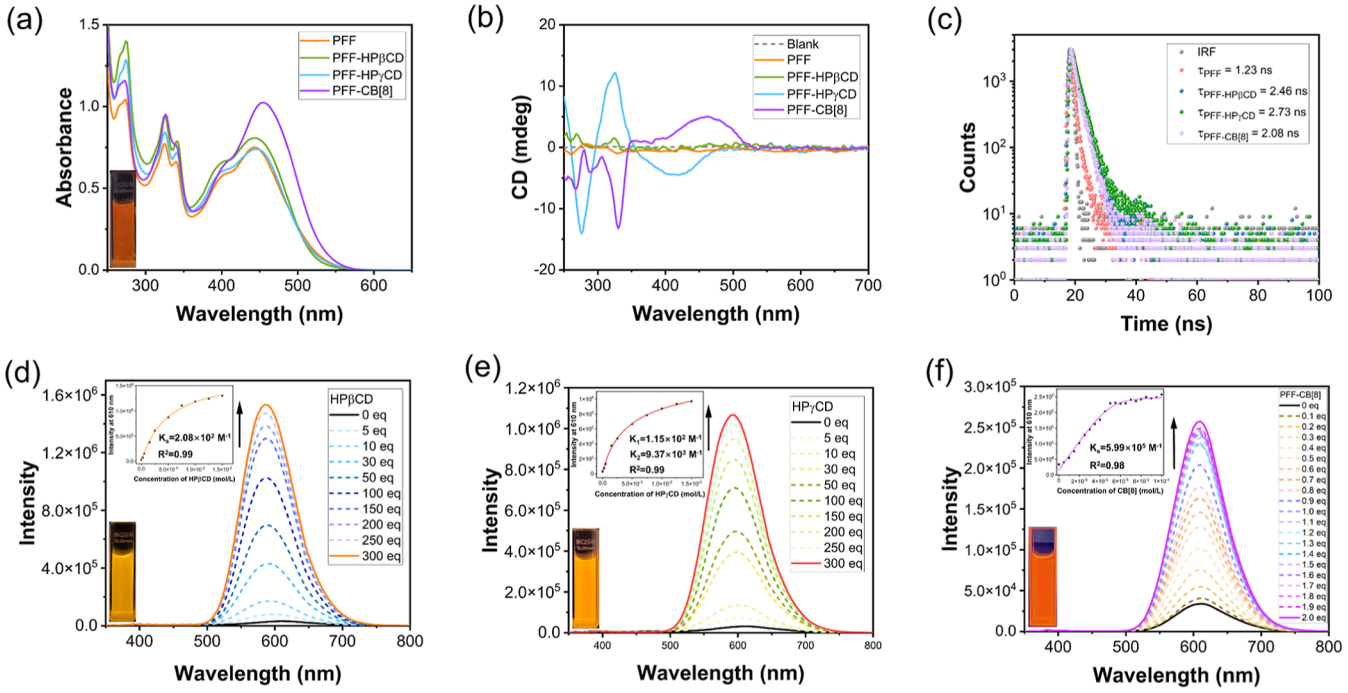

Figure 1. (a) UV−vis absorbance (inset: the photo of PFF solution under 365 nm UV irradiation), (b) CD spectra, and (c) time-resolved decay spectra of PFF, PFF-HPβCD, PFF-HPγCD, and PFF-CB[8] in H_2O/DMSO (99:1, v/v, [PFF] = [CB[8]] = 5×10^{-5} M, [HPβ/γCD] = 1.5×10^{-2} M); the fluorescence titration spectra of PFF with the addition of (d) HPβCD, (e) HPγCD, and (f) CB[8] (inset: the corresponding fluorescence emission intensity changes of PFF at 610 nm in the presence of the hosts and photos of three assembly solutions under 365 nm UV irradiation).

the fluorescence titration spectra exhibited a persistent blue-shift from 610 to 585 nm and a 50-fold fluorescence enhancement with a QY of 42.49% and a lifetime of 2.46 ns until stabilizing around 300 equiv HPβCD (Figure S11), which was attributed to restricted fluorophore vibration and reduced aggregation. Job's plot of PFF and HPβCD indicated a 1:1 stoichiometric ratio (Figure S12a), and the binding constant (K_s) was calculated to be 2.08×10^2 M^{-1} by the nonlinear least-squares fitting method. ^{1}H NMR experiments also confirmed the binding behavior between PFF and HPβCD, in which the proton signals on the pyrene group occurred during the peak passivation and a high-field shifting (Figure S13). Different from HPβCD, HPγCD with a larger cavity could encapsulate PFF at stoichiometric ratios of 1:2 as determined by the Job's plot and gave a higher K_s to be 1.08×10^6 M^{-2} (Figures 1e and S11b), which further confirmed the stronger binding ability by ^{1}H NMR titration (Figure S14). The 2D NOESY spectra of PFF-HPβ/γCD presented the correlation signal between protons on the pyrene units and HPβ/γCD (Figure S15), which further confirmed the formation of supramolecular assemblies. The fluorescence intensity of PFF enhanced 35-fold and blue-shifted to 595 nm, achieving the QY of 32.14% and a lifetime of 2.73 ns when 300 equiv of HPγCD were added (Figure S16). The use of 300 equiv HPβ/γCD to construct supramolecular assemblies was to ensure that the PFF molecules were completely encapsulated, thereby maximizing the disruption of their own $\pi-\pi$ stacking and ACQ effect and then achieving the best fluorescence enhancement effect. We determined the QYs of PFF-HPβCD (1:1) and PFF-HPγCD (2:1) under the optimal stoichiometric ratio, which were 4.32% and 6.93%, respectively (Figure S17). Moreover, the QYs of PFF-HPβ/γCD at even higher host concentrations (350 and 500 equiv) were slightly lower than those at 300 equiv (Figures S18 and S19), which was consistent with our expectations. On the other hand, the fluorescence titration experiment revealed that the complexation between CB[8] and PFF at a 1:1 stoichiometric ratio showed a high K_s up to 5.99×10^5 M^{-1} attributed to both strong ionic dipole interaction and hydrophobic interaction (Figures 1f and S12c). The PFF-CB[8] assembly displayed a 7-fold fluorescence increase at 610 nm with a QY of 34.10% and a lifetime of 2.08 ns, as shown in Figures 1c and S20. ^{1}H NMR spectroscopy showing a low-field-shift of the protons on the vinyl phenylpyridine and a high-field-shift of the protons on pyrene further supported the strong interaction, which also indicated the CB[8] bound to the positive charge site of PFF and the pyrene moiety was outside the cavity (Figure S21). According to previous reports,[37] the internal diameters of HPβCD and HPγCD are approximately 5.8−7.8 Å and 7.4−9.5 Å, respectively, which explains that HPγCD can bind to two PFF molecules. However, CB[8] has a portal diameter of 6.9 Å and tends to bind a cationic vinyl phenylpyridine moiety via ion−dipole interactions with carbonyl groups. To confirm that the host−guest enhancement is not solvent-specific, fluorescence spectra were further collected in H_2O/DMF (99:1, v/v) and H_2O/MeOH (99:1, v/v). In both mixed solvents, PFF retained the ACQ behavior, and the addition of HPβCD, HPγCD, or CB[8] produced pronounced fluorescence enhancement due to macrocyclic confinement (Figure S22), consistent with the results in H_2O/DMSO (99:1, v/v). In addition, HPβ/γCD and CB[8] exhibited no fluorescence within the emission range of PFF as shown in Figure S23, confirming that the observed fluorescence enhancement was entirely due to the formation of supramolecular complexes between PFF and the three hosts.

https://doi.org/10.1021/jacsau.5c01631
JACS Au 2026, 6, 621−630

After the binding models and behaviors of macrocyclic confinement were studied, their topological aggregation morphologies were revealed through transmission electron microscopy (TEM) experiments. As shown in Figure 2, the

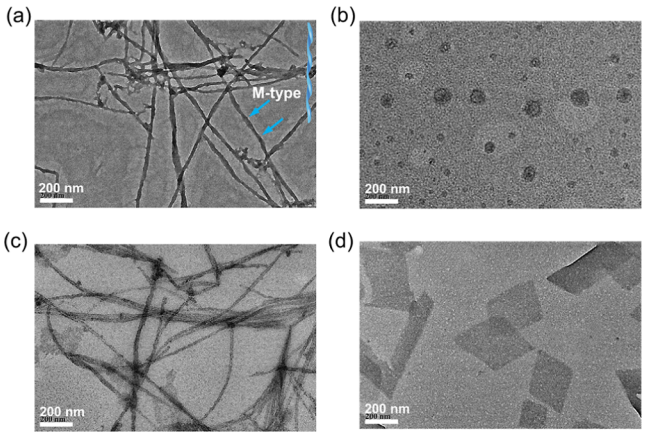

Figure 2. TEM images of (a) PFF, (b) PFF-HPβCD, (c) PFF-HPγCD, and (d) PFF-CB[8] ([PFF] = [CB[8]] = 5×10^{-5} M, [HPβ/γCD] = 1.5×10^{-2} M).

free guest PFF molecules led to *M* rotational nanofibers attributed to the $\pi-\pi$ stacking of pyrene groups, which has been supported by MD calculations. In comparison, the PFF-HPβCD supramolecular assembly transformed into spherical nanoparticles with diameters ranging from 50 to 100 nm, and PFF-HPγCD formed fine nanotubes with a diameter of approximately 20 nm. Interestingly, the morphology of PFF-CB[8] exhibited rectangular nanosheets in the TEM image. From the above experimental results, HPβ/γCD and CB[8] possessed different binding affinities and bonding positions with PFF, which not only effectively expanded the fluorescence emission of PFF but also realized a diverse regulation of the topological morphology of the aggregates.

Although free PFF self-assembled to form helical nanofibers, no obvious CD signals were observed in the range 350−600 nm (Figure 1b). PFF-HPβCD also exhibited negligible Cotton effect peaks because of its relatively weak bonding ability. Interestingly, HPγCD gave rise to a negative CD signal at 440 nm corresponding to chirality transfer from FF to the pyrene group, and the asymmetric factor (g_{abs}) was calculated as -1.44×10^{-4} (Figure 1b). This phenomenon aligned with the DFT studies in which two PFFs were encapsulated within the cavity of HPγCD in a head-to-head configuration (Figure 3a). In comparison, the PFF-CB[8] assembly showed a positive CD signal at 450 nm with a notable g_{abs} calculated as $+1.42 \times 10^{-4}$ (Figure 1b). No Cotton effect peak value of 350−600 nm has been found for any of the assemblies in nonpolar DMSO (Figure S24), and the absence of CD signals could be attributed to the very weak host−guest interaction between the macrocycles and PFF in DMSO. The above results confirmed that macrocyclic confinement via hydrophobic and electrostatic interactions played a critical role in inducing chiral transmission in the supramolecular PFF assemblies. As a control experiment, we synthesized 1-methyl-4-(2-(pyren-1-yl-vinyl)-pyridinium iodide (PY) without the phenylalanine dipeptide moiety (FF) characterized by NMR and HR-MS experiments (Figures S4−S6). Although spectral titration experiments confirmed that HPβ/γCD and CB[8] could encapsulate PY by host−guest complexation (Figures S25−S33), the addition of macrocycles induced no obvious chiral signals of PY in the range 350−600 nm (Figure S34), which implied that the macrocyclic cavity cannot directly induce obvious chirality of the pyrene moiety. The further doping of FF emerged no Cotton effect peaks corresponding to the UV/vis signal of PY, indicating that the noncovalent assembly with FF could not achieve chiral transfer to PY. Collectively, these results demonstrated that macrocyclic confinement enabled PFF single-molecule efficient chirality transferred from the FF to the pyrene group.

To further explore the origin of chirality transfer, DFT calculations and MD simulations were performed. The results showed that the HOMO-LUMO energy gap of free PFF was 2.84 eV, while complexation with macrocycles resulted in narrowed gaps (Figure 3a). Notably, PFF-HPγCD and PFF-CB[8] exhibited reduced gaps of 2.56 and 2.13 eV, indicating macrocyclic encapsulation effectively stabilized the frontier orbitals and facilitated photoexcitation, thereby leading to enhanced luminescent behaviors. The markedly deeper LUMO of the PFF-CB[8] complex arises from the much stronger ion−dipole electrostatic interaction between CB[8] and the positively charged pyridinium unit of PFF, which stabilizes the frontier orbitals more effectively than cyclodextrin encapsulation.[38]

To gain deeper insights into the chiroptical behavior, 200 PFF molecules were simulated in an aqueous solution using MD. Within 10 ns, all PFF dimers with an intermolecular distance of 5 Å and an interplanar angle less than 10° were identified. Spontaneous $\pi-\pi$ stacking led to the formation of 46 stable pyrene−pyrene dimers (Figure 3b,e), indicating a strong tendency of aggregation in aqueous media. As the simulation progressed to 100 ns, the molecules further formed helical stacks around the pyrene moieties, which was consistent with the observed results for *M* rotational nanofibers of PFF in the TEM image (Figure 3c). Molecular simulation indicated that at an early stage of assembly, most PFF molecules formed dimers with a parallel, symmetric head-to-head manner (Figure 3d). These dimers adopted a broad distribution of twist angles indicating low overall chirality. MD simulations in a 1% DMSO−H_2O mixture (100 ns) showed similar dimer formation and aggregation patterns as in pure water, indicating that the small DMSO content has a minimal influence on the overall assembly behavior (Figure S35). Subsequent ECD calculations on the PFF aggregate extracted from the MD trajectories revealed negligible Cotton effects (Figure S36), confirming that the PFF aggregates eliminated chiral exciton coupling. These computational findings were consistent with the experimental CD spectra of PFF. Meanwhile, ECD calculations showed that PFF-HPγCD and PFF-CB[8] assemblies exhibited pronounced and distinct Cotton effects, whereas PFF-HPβCD displayed a weak CD signal, likely due to its lower binding affinity (Figure S37). In case of HPγCD, two PFF molecules were asymmetrically aligned around its chiral cavity, which suppressed the achiral aggregation and stabilized the CD-active conformer. For CB[8], the strong host−guest interaction at a 1:1 stoichiometric ratio posed strong conformational restrictions on PFF, disrupting the pyrene−pyrene stacking and resulting in chiroptical activity. This interaction biased the chromophore toward twisted configurations with net chirality. Collectively, these findings highlight two key mechanisms by which macrocycle-confined guests lead to chirality transmission: (i) disruption of achiral

https://doi.org/10.1021/jacsau.5c01631
JACS Au 2026, 6, 621−630

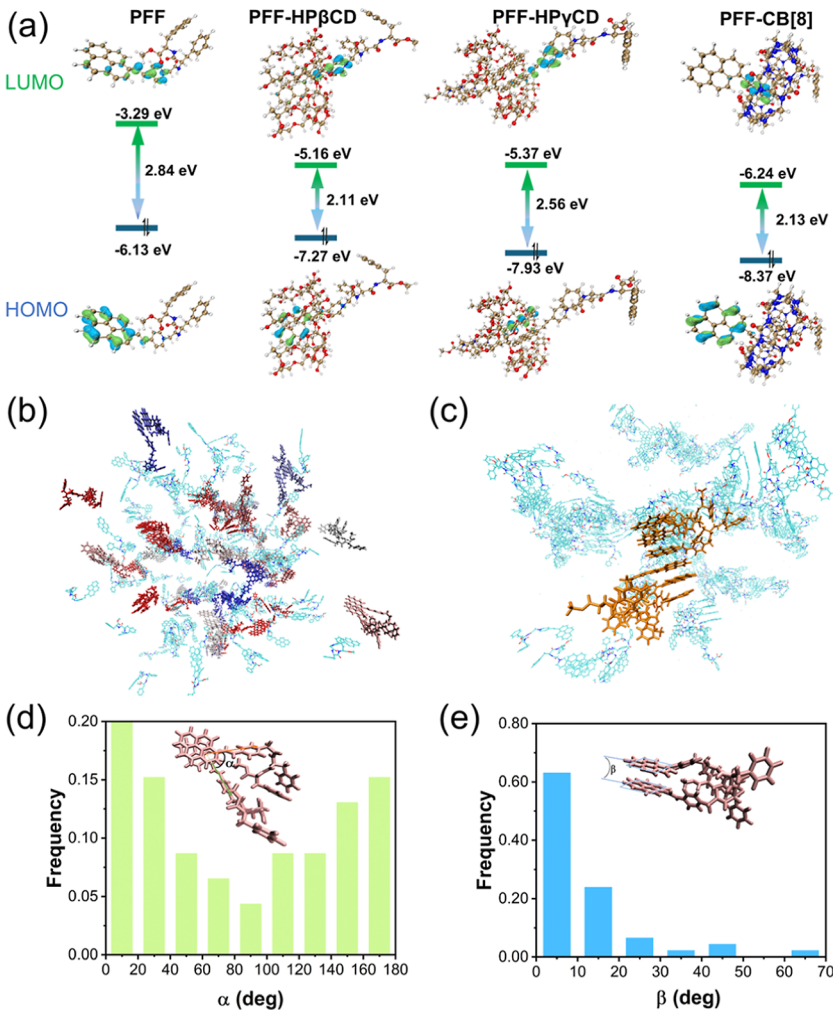

Figure 3. (a) HOMO−LUMO analyses illustrating the real-space distributions of holes (blue) and electrons (green), along with energy level diagrams for PFF, PFF-HPβCD, PFF-HPγCD, and PFF-CB[8]; (b) final snapshot from a 10 ns MD simulation of 200 PFF molecules in an aqueous solution (representative pyrene dimers are color-coded and all other molecules are depicted in cyan); (c) final frame from a 100 ns GROMACS MD simulation of the PFF system (molecular exhibiting pyrene−pyrene stacking interactions are highlighted in yellow for clarity); histograms of (d) intermolecular twist angle α; and (e) interplanar angle β parameters for all detected dimers from 10 ns simulation.

aggregation pathways and (ii) stabilization of chiral conformers through geometric confinement.

As can be seen from the above CD spectroscopic and theoretical studies, it is indicative that the chiral transfer can be attributed to macrocyclic confinement. Due to the weak nature of the host−guest interaction, we wanted to investigate the temperature-responsive assembly and disassembly of PFF-HPγCD and PFF-CB[8]. As illustrated in Figures 4 and S38, the negative Cotton effect peak of PFF-HPγCD at 440 nm realized strong and reversible temperature-controlled chiral transfer with the increase or decrease of temperature (20−75 °C). Concomitantly, the morphology of PFF-HPγCD exhibited nanoparticles at 75 °C in TEM images and reverted to nanotubes when it was cold down to 20 °C (Figure S39). Unlike the PFF-HPγCD complex, the temperature only placed a minor effect on the PFF-CB[8]'s CD signal at 450 nm due to its ionic dipole electrostatic interaction further stabilizing the complexation. The CD spectroscopy research indicated that the macrocyclic confinement achieved reversible temperature-controlled supramolecular chiral transfer switches. However, the chirality of PFF-HPβCD showed no obvious change with thermal stimulation because of weak complexation. Subsequently, we further explored the influence of temperature variations on the luminescence performance of supramolecular chiral switches' luminescence performance. The fluorescence of PFF-HPβCD and PFF-HPγCD greatly decreased with the temperature increasing, and the quenching efficiencies were 64.84% and 55.59%, respectively. The fluorescence emission of PFF-CB[8] with a stronger bonding effect diminished by 37.97% as the temperature rose to 75 °C. As the temperature of the system gradually decreased, the fluorescence intensities gradually recovered (Figure S40). After studying their temperature responsiveness, we further discovered that supramolecular chiral assemblies PFF-HPγCD and PFF-CB[8] possessed CPL behaviors. As shown in Figure 5a, b, PFF-HPγCD gave a positive CPL signal corresponding to its fluorescence emission in the 500−800 nm range, and the g_{lum} value was 1.30×10^{-4}, and the PFF-CB[8] also generated a positive CPL signal with a g_{lum} value of 1.28×10^{-4}, which indicated that the CPL was derived from the chiral transfer based on macrocyclic confinement.

The supramolecular chiral transfer switches with thermally reversible response performance realized the regulation of multistate chiral assemblies, which was successfully applied in a

https://doi.org/10.1021/jacsau.5c01631
JACS Au 2026, 6, 621−630

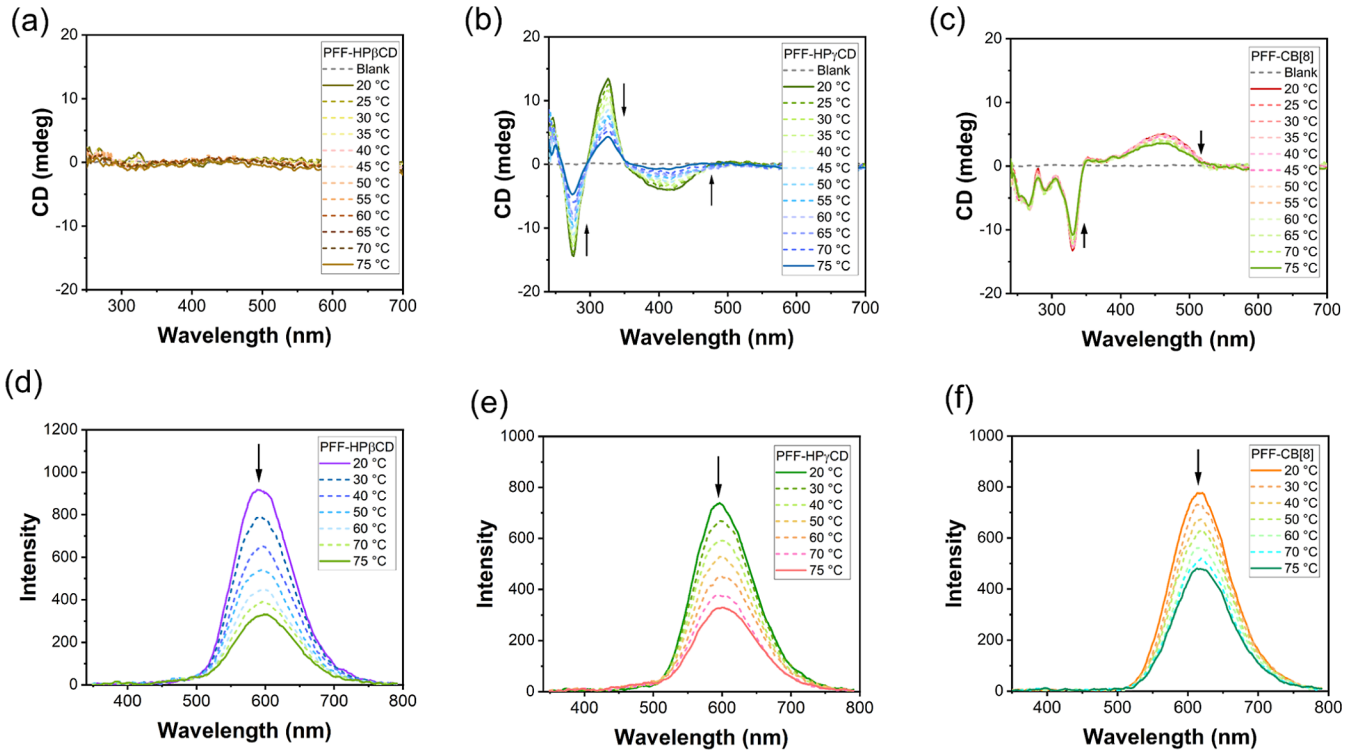

Figure 4. CD spectra of (a) PFF-HPβCD, (c) PFF-HPγCD, and (e) PFF-CB[8] and the fluorescence spectra of (b) PFF-HPβCD, (d) PFF-HPγCD, and (f) PFF-CB[8] under heating conditions from 20 to 75 °C in H_2O/DMSO (99:1, v/v, [[PFF] = [CB[8]] = 5×10^{-5} M, [HPβ/γCD] = 1.5×10^{-2} M).

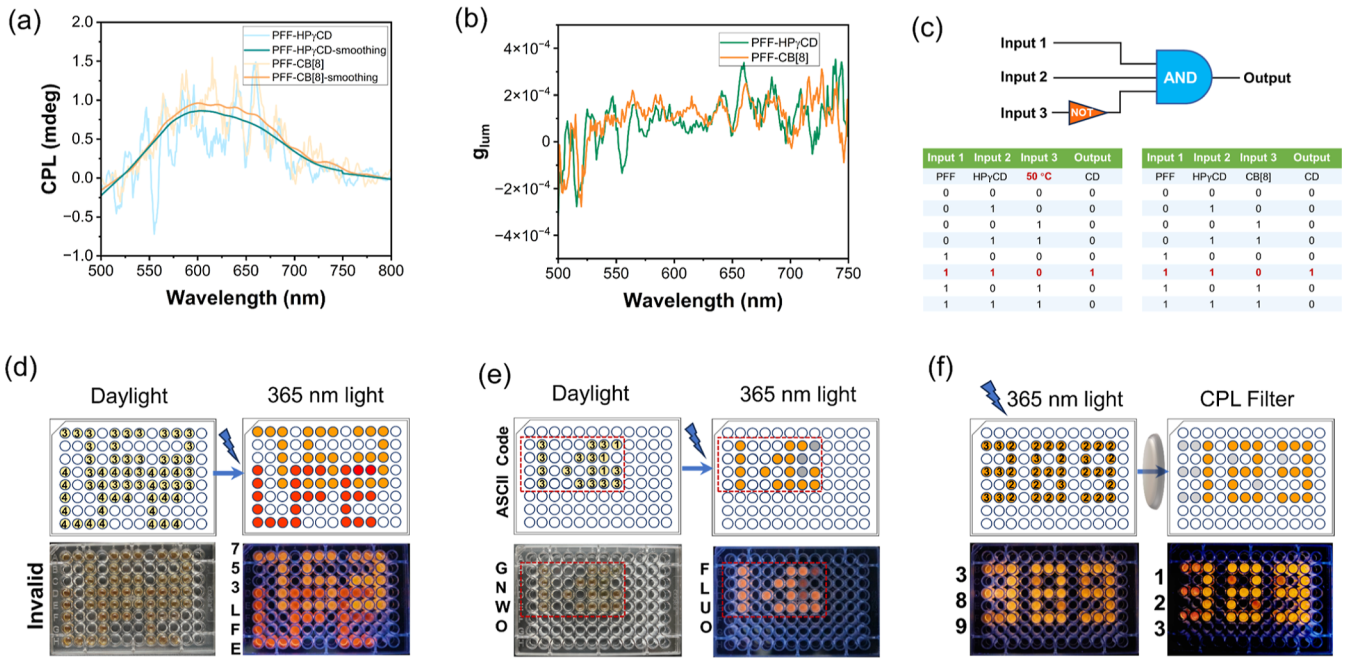

Figure 5. CPL spectra (a) and g_{lum} (b) of PFF-HPγCD and PFF-CB[8] in H_2O/DMSO (99:1, v/v); (c) temperature (50 °C) or CB[8] regulated and INHIBIT logic gate; (d) schematic illustration of information encryption under daylight and 365 nm light; (e) binary information encryption according to the 8-bit ASCII Code; and (f) CPL filter information encryption. ([PFF] = [CB[8]] = 5×10^{-5} M, [HPβ/γCD] = 1.5×10^{-2} M. ①: PFF, ②: PFF-HPβCD, ③: PFF-HPγCD, ④: PFF-CB[8]. The four solutions were added to the 96-well plate, respectively).

chiral logic gate and multilayer chiral information anticounterfeiting system. As shown in Figures 5c and S42, the components of PFF, HPγCD, and temperature or CB[8] were defined as "Input". The CD signal intensity at 420 nm below −3 was denoted as "1" for "Output", while values above −3 were labeled "0". In this logic gate system, temperature or CB[8] was utilized as a nongate to "mute" the output signal clearly displaying in the truth table, and the CD intensity at 420 nm can "lock" the supramolecular assembly of PFF-HPγCD, which demonstrated molecular-level information

https://doi.org/10.1021/jacsau.5c01631
JACS Au 2026, 6, 621−630

processing driven by supramolecular chirality. The macrocycle-confined supramolecular chiral assemblies with excellent luminescent properties can also realize multilevel information encryption. As seen from 96-well plates, PFF-CB[8] emitted bright orange-red fluorescence, and PFF-HPγCD appeared yellow under 365 nm irradiation, allowing the direct visualization of numbers ("752") and letters ("LFE") via spatial fluorescence contrast, whereas there was no effective information under daylight because the all wells appeared visually identical (Figure 5d). Furthermore, the binary pattern followed the 8-bit ASCII encoding of each character with fluorescence intensity serving as the binary state (1 = ON, 0 = OFF). The message "GNWO" was displayed under daylight, while under UV light, it revealed "FLUO" by using wells containing either PFF alone or with HPγCD (Figures 5 and S43). Especially, we further leveraged the difference in CPL output between PFF-HPγCD and PFF-HPβCD to construct a polarization-dependent encryption system (Figures 5f and S44). Under unfiltered UV, a "389" pattern was visible. Upon applying a left-handed CPL filter, the reduced emission of the PFF-HPγCD complex led to a different readout "123", thereby revealing a hidden layer of chiroptical information only under specific polarization conditions. Macrocycle-mediated chirality transfer has been successfully applied in the multilevel information counterfeit and polarization-dependent encryption.

CONCLUSION

In summary, we constructed a series of morphology-tunable aggregates and temperature-controlled supramolecular chiral switches based on PFF through macrocyclic modulation. HPβCD, HPγCD, and CB[8], respectively, encapsulating PFF not only tuned the topological transformation of PFF from helical nanofibers to spherical nanoparticles, fine nanotubes, and rectangular nanosheets but also displayed significant fluorescence enhancement with QY increasing from 1.66% of PFF to 42.49%, 32.14%, and 34.10%, respectively. Especially, PFF-HPγCD and PFF-CB[8] with higher binding effects effectively disrupted the $\pi-\pi$ stacking of PFF into symmetric aggregates and restricted conformations achieving chiral transmission, displaying a negative Cotton effect peak at 440 nm ($g_{abs} = -1.44 \times 10^{-4}$) and a positive CD signal at 450 nm ($g_{abs} = +1.42 \times 10^{-4}$), respectively, which was further confirmed by MD and DFT theoretical calculation. Meanwhile, under the thermal stimulation ranging from 20 to 75 °C, PFF-HPγCD and PFF-CB[8] as chiral switches exhibited reversible responsive chiral signals of varying degrees and emitted positive CPL signals corresponding to their fluorescence peaks. Especially, the supramolecular chiral temperature switches were successfully applied in advanced logic gate systems and polarization-dependent CPL encryption.

EXPERIMENTAL SECTION

Materials

The chemicals and solvents were purchased from commercial suppliers.[39] All reagents were used without purification, unless specified otherwise.

Measurements

^{1}H NMR and ^{13}C NMR spectra were performed on the Bruker DMX spectrometer at 298 K. High-resolution mass spectra (HRMS) were recorded on a 6520 Q-TOF LC/MS (Agilent). The UV−vis absorption spectra were recorded on a Thermo Fisher Scientific EVO300 PC spectrophotometer (light path of the quartz cell = 1 cm). The fluorescence spectra, quantum yields, and time-correlated decay profiles were accomplished on the Edinburgh Instrument FS5 spectrometer (Livingstone, UK).[40] The CD spectra were recorded on a BioLogic MOS-500. The CPL spectra were performed on the JASCO CPL-300. The Commission International del' Eclairage (CIE) 1931 chromaticity diagram was determined by FLS1000 software. TEM experiments were performed on an FEI Tecnai G2 F20 (200 kV). Photographs under UV irradiation and through a circular polarizer were taken using a Sony A7R III mirrorless digital camera equipped with a 35−75 mm f/1.8 lens. A Kase CPL filter was mounted in front of the lens for chiroptical contrast imaging. The CPL filter has a polarization extinction ratio of 100:1 (20 dB) and a measurement uncertainty of less than 1%. All images were captured under identical exposure settings to ensure comparability across the experimental conditions.

Molecular Dynamics Simulations

All molecular dynamics (MD) simulations were performed by using the GROMACS 2022.3 software package. The bonded and non-bonded interaction parameters of the PFF molecule and HPγCD were derived from the second-generation General Amber Force Field (GAFF2). Missing bonded parameters were completed using the parmchk2 utility, and restrained electrostatic potential (RESP) charges were computed using the Multiwfn 3.8 program39 based on gas-phase geometries optimized at the B3LYP/6-31G(d) level.

To ensure proper thermalization and equilibration, the systems underwent sequential annealing consisting of 10 cycles of the NVT (constant number, volume, and temperature) ensemble at 300 K and 10 cycles of the NPT (constant number, pressure, and temperature) ensemble at 1 bar, each cycle lasting 2 ns. Following annealing, production MD simulations were conducted for 10, 25, and 50 ns depending on the system. The temperature was maintained using a velocity-rescaled (V-rescale) thermostat, and pressure was controlled with the Berendsen barostat.

All simulations used a 2 fs time step with all covalent bonds involving hydrogen atoms constrained via the LINCS algorithm. Nonbonded van der Waals and short-range electrostatic interactions were calculated using a cutoff of 1.0 nm, while long-range electrostatics were treated using the particle-mesh Ewald method. Snapshots from the final 50 ns trajectories were extracted for structural and statistical analyses, including aggregation behavior and host−guest geometries.

Time-Dependent Density Functional Theory Calculations

To investigate the chiroptical properties of PFF monomers and host−guest complexes, geometry optimizations and ECD calculations were performed using a multistep approach. Initial conformational sampling was carried out using GROMACS-based molecular dynamics simulations followed by clustering and energy minimization to identify low-energy conformers. For each system, the five lowest-energy conformers were selected for ECD calculations, and the final spectrum was obtained by the Boltzmann-weighted averaging of individual ECD spectra.

All gas-phase ground-state geometries were optimized at the DFT level using the B3LYP functional[41] with the def2-SVP basis set,[42] incorporating Grimme's D3 dispersion correction with Becke-Johnson damping (D3BJ).[43] Harmonic vibrational frequency calculations were performed to confirm that each optimized structure corresponded to a local minimum on the potential energy surface (no imaginary frequencies).

Subsequent TD-DFT calculations were conducted using the CAM-B3LYP functional[44] and the same def2-SVP basis set. Vertical excitations were computed from the optimized ground-state geometries, including the first 20 singlet excited states, and both electric and magnetic transition dipole moments were used to simulate the ECD spectra.

All DFT and TD-DFT computations were performed using the Gaussian 16 program suite.[45]

https://doi.org/10.1021/jacsau.5c01631
JACS Au 2026, 6, 621−630

Synthesis of Compound PFF

Compounds **1**[46] and **FF**[47] (Scheme S1) were synthesized according to the previous reports. **1** (50 mg, 0.16 mmol) and FF (88 mg, 0.19 mmol) were added to CH_3CN (15 mL). The mixture was heated to 85 °C and kept refluxing overnight under a nitrogen atmosphere. Then, diethyl ether was poured into the reaction mixture to obtain orange precipitate and dried under vacuum to give PFF (83 mg, yield: 67%).

^{1}H NMR (400 MHz, DMSO-d_6, 298 K): δ 9.15 (d, J = 15.9 Hz, 1H), 8.96 (d, J = 9.3 Hz, 1H), 8.92 (d, J = 8.4 Hz, 1H), 8.76 (d, J = 7.7 Hz, 1H), 8.71 (d, J = 6.6 Hz, 2H), 8.68 (d, J = 8.4 Hz, 1H), 8.51 (d, J = 6.6 Hz, 2H), 8.41 (t, J = 8.1 Hz, 4H), 8.31 (d, J = 9.0 Hz, 1H), 8.26 (d, J = 8.8 Hz, 1H), 8.15 (t, J = 7.6 Hz, 1H), 7.87 (d, J = 15.8 Hz, 1H), 7.29−7.23 (m, 5.2 Hz, 10H), 5.29 (d, J = 3.4 Hz, 2H), 4.70−4.62 (m, 1H), 4.55−4.49 (m, 1H), 3.61 (s, 3H), 3.05 (m, 2H), 2.95 (m, 1H), 2.79 (m, 1H). ^{13}C NMR (100 MHz, DMSO-d_6, 298 K): δ 171.60, 170.53, 164.10, 153.34, 145.35, 137.42, 137.14, 137.00, 132.39, 130.87, 130.26, 129.55, 129.29, 129.03, 128.93, 128.84, 128.60, 128.27, 128.11, 127.37, 126.73, 126.60, 126.40, 126.31, 126.03, 125.66, 125.45, 124.30, 124.16, 123.73, 123.62,123.09, 60.55, 53.94, 53.71, 51.90, 38.10, 36.59. HR-MS (ESI) m/z: calcd for $C_{44}H_{38}N_3O_4^-$ [PFF-Br]$^-$, 627.286; found, 627.286.

Synthetic Route of PY

Compound PY was synthesized according to the previous reports.[48]

^{1}H NMR (400 MHz, DMSO-d_6, 298 K): δ 9.11 (d, J = 16.1 Hz, 1H), 8.96 (d, J = 9.4 Hz, 1H), 8.93 (d, J = 7.0 Hz, 2H), 8.66 (d, J = 8.3 Hz, 1H), 8.51 (d, J = 7.0 Hz, 2H), 8.40 (t, J = 8.4 Hz, 4H), 8.28 (d, J = 11.5 Hz, 2H), 8.16 (t, J = 7.6 Hz, 1H), 7.85 (d, J = 16.0 Hz, 1H), 4.30 (s, 3H). ^{13}C NMR (100 MHz, DMSO-d_6, 298 K): δ 152.44, 145.04, 136.65, 132.29, 130.90, 130.29, 129.46, 128.99, 128.76, 128.56, 127.40, 126.74, 126.41, 126.28, 126.00, 125.71, 125.47, 124.20, 123.94, 123.77, 123.13. HR-MS (ESI) m/z: calcd for $C_{24}H_{18}N^-$ [PY-I]$^-$, 320.143; found, 320.143.

Preparation of Supramolecular Assemblies

PFF was dissolved in DMSO at a concentration of 3×10^{-3} M. HPβ/γCD was dissolved in water at a concentration of 3×10^{-3} M. CB[8] was dissolved in water at a concentration of 1×10^{-4} M. According to the required concentration for the experimental test, the above host and guest solutions were taken and mixed in H_2O/DMSO (99:1, v/v). Ensure thorough mixing by vortexing and ultrasonication and then let them stand at 25 °C for 30 min before conducting all the characterizations.

■ ASSOCIATED CONTENT

Supporting Information

The Supporting Information is available free of charge at https://pubs.acs.org/doi/10.1021/jacsau.5c01631.

Synthesis route, NMR and MS spectra, UV−vis spectra, fluorescence spectra, quantum yields, job plots, ^{1}H NMR titration spectra, 2D NOESY spectra, CD spectra, fluorescence titration spectra, UV−vis titration spectra, time-resolved decay spectra, MD simulation, ECD calculation spectra, TEM images, 8-bit ASCII Code, and CPL spectra (PDF)

■ AUTHOR INFORMATION

Corresponding Authors

Xuejian Zhang − *College of Chemistry, State Key Laboratory of Elemento-Organic Chemistry, Nankai University, Tianjin 300071, P. R. China*; Email: 9820230017@nankai.edu.cn

Yu Liu − *College of Chemistry, State Key Laboratory of Elemento-Organic Chemistry, Nankai University, Tianjin 300071, P. R. China*; orcid.org/0000-0001-8723-1896; Email: yuliu@nankai.edu.cn

Authors

Xuan Zhao − *College of Chemistry, State Key Laboratory of Elemento-Organic Chemistry, Nankai University, Tianjin 300071, P. R. China*

Shuangqi Song − *College of Chemistry, State Key Laboratory of Elemento-Organic Chemistry, Nankai University, Tianjin 300071, P. R. China*

Hengzhi Zhang − *College of Chemistry, State Key Laboratory of Elemento-Organic Chemistry, Nankai University, Tianjin 300071, P. R. China*

Complete contact information is available at: https://pubs.acs.org/10.1021/jacsau.5c01631

Author Contributions

X. Z., S. S., and H. Z. synthesized the compounds and performed the experiments. X. Z. summarized and collected data and wrote the manuscript. The work was supervised by X.-J. Z and Y. L. All authors have given approval to the final version of the manuscript.

Funding

This study was funded by the National Natural Science Foundation of China (22131008) and the Tianjin Key Research and Development Program (Grant no. 25YFYFFG01420).

Notes

The authors declare no competing financial interest.

■ ACKNOWLEDGMENTS

The authors thank the National Nature Science Foundation of China (NNSFC, Grant Nos. 22131008), the Tianjin Key Research and Development Program (Grant No. 25YFYFFG01420), and China Fundamental Research Funds for the Central Universities for financial support.

■ ABBREVIATIONS

HPβ/γCD, β/γcyclodextrin remdummy; CB[8]remdummy, cucurbit[8]uril; PFFremdummy, phenylalanine dipeptide-modified pyrene; FFremdummy, phenylalanine dipeptide; PYremdummy, 1-methyl-4-2-(pyren-1-yl-vinyl)-pyridinium iodide; DMSOremdummy, dimethyl sulfoxide; $K_s$remdummy, binding constant; CDremdummy, circular dichroism; CPLremdummy, circularly polarized luminescence; QYremdummy, quantum yield; MDremdummy, molecular dynamics; ECDremdummy, electronic circular dichroism; DFTremdummy, density functional theory; NMRremdummy, nuclear magnetic resonance; HR-MSremdummy, high-resolution mass spectrometry; ACQremdummy, aggregation-caused quenching; 2D NOESYremdummy, two-dimensional nuclear Overhauser effect spectroscopy; TEMremdummy, transmission electron microscopy.

■ REFERENCES

(1) Suzuki, Y.; Mizuta, Y.; Mikagi, A.; Misawa-Suzuki, T.; Tsuchido, Y.; Sugaya, T.; Hashimoto, T.; Ema, K.; Hayashita, T. Recognition of d-Glucose in Water with Excellent Sensitivity, Selectivity, and Chiral Selectivity Using γ-Cyclodextrin and Fluorescent Boronic Acid Inclusion Complexes Having a Pseudo-diboronic Acid Moiety. *ACS Sens.* **2023**, *8*, 218−227.

(2) Yu, H.; Hao, A.-Y.; Xing, P.-Y. Dynamically Folded Chiral Arms for Selectively Clamping Aromatic Imides. *Nano Lett.* **2025**, *25*, 3357−3366.

(3) Sun, G.; Zhang, X.; Zheng, Z.; Zhang, Z.-Y.; Dong, M.; Sessler, J. L.; Li, C. Chiral Macrocycles for Enantioselective Recognition. *J. Am. Chem. Soc.* **2024**, *146*, 26233−26242.
(4) Ouyang, J.; Swartjes, A.; Geerts, M.; Gilissen, P. J.; Wang, D.; Teeuwen, P. C. P.; Tinnemans, P.; Vanthuyne, N.; Chentouf, S.; Rutjes, F. P. J. T.; et al. Absolute Configuration and Host-guest Binding of Chiral Porphyrin-cages by a Combined Chiroptical and Theoretical Approach. *Nat. Commun.* **2020**, *11*, 4776.
(5) Fredy, J. W.; Méndez-Ardoy, A.; Kwangmettatam, S.; Bochicchio, D.; Matt, B.; Stuart, M. C. A.; Huskens, J.; Katsonis, N.; Pavan, G. M.; Kudernac, T. Molecular Photoswitches Mediating the Strain-driven Disassembly of Supramolecular Tubules. *Proc. Natl. Acad. Sci. U.S.A.* **2017**, *114*, 11850−11855.
(6) Erbas-Cakmak, S.; Leigh, D. A.; McTernan, C. T.; Nussbaumer, A. L. Artificial Molecular Machines. *Chem. Rev.* **2015**, *115*, 10081−10206.
(7) Yu, J.; Yu, H.; Qiu, Y.; Zhang, H.-Y.; Xu, X.; Liu, Y. Biofuel-Driven Stepping Chiral Supramolecular Transfer Container. *Angew. Chem., Int. Ed.* **2025**, *137*, No. e202418938.
(8) Li, M.; Chen, L.-J.; Cai, Y.; Luo, Q.; Li, W.; Yang, H.-B.; Tian, H.; Zhu, W.-H. Light-Driven Chiral Switching of Supramolecular Metallacycles with Photoreversibility. *Chem.* **2019**, *5*, 634−648.
(9) Qi, W.; Ma, C.; Yan, Y.; Huang, J. Chirality manipulation of supramolecular self-assembly based on the host-guest chemistry of cyclodextrin. *Curr. Opin. Colloid Interface Sci.* **2021**, *56*, 101526.
(10) Wang, X.-J.; Zhi, W.-W.; Ma, C.; Zhu, Z.-Y.; Qi, W.-L.; Huang, J.-B.; Yan, Y. Not by Serendipity: Rationally Designed Reversible Temperature Responsive Circularly Polarized Luminescence Inversion by Coupling Two Scenarios of Harata-Kodaka's Rule. *JACS Au* **2021**, *1*, 156−163.
(11) Liang, B.; Cheng, Y.; Ma, J.; Jia, L.; Zheng, Q.; Wang, P.; Xia, D. A Chiral Supramolecular Liquid Crystal Based on Pillararene and its Application in Information Encryption. *Chem. Commun.* **2024**, *60*, 12698−12701.
(12) Zhou, B.; Yang, X.; Liu, J.-Z.; Lan, L.-D.; Lu, H.; Wang, Y.-Y.; Wei, Z.-B.; Zhang, X.-X. Jellyfish-Inspired Self-Healing Luminescent Elastomers Based on Borate Nanoassemblies for Dual-Model Encryption. *Nano Lett.* **2024**, *24*, 8198−8207.
(13) Zhao, X.; Zhou, X.; Xing, W.-W.; Liu, Y. Triazine Pyridinium Derivative Supramolecular Cascade Assembly Extended FRET for Two-photon NIR Targeted Cell Imaging. *Chem. Commun.* **2023**, *59*, 11516−11519.
(14) Lou, X.-Y.; Zhang, K.; Bai, Y.; Zhang, S.; Li, Y.; Yang, Y.-W. Self-Assembled Nanohelixes Driven by Host-Guest Interactions and Metal Coordination. *Angew. Chem., Int. Ed.* **2025**, *137*, No. e202414611.
(15) Zhang, W.; Zhang, Y.-M.; Li, S.-H.; Cui, Y.-L.; Yu, J.; Liu, Y. Tunable Nanosupramolecular Aggregates Mediated by Host−Guest Complexation. *Angew. Chem., Int. Ed.* **2016**, *55*, 11452−11456.
(16) Wu, Y.; Sun, L.; Chen, X.; Liu, J.; Ouyang, J.; Zhang, X.; Guo, Y.; Chen, Y.; Yuan, W.; Wang, D.; et al. Cucurbit[8]uril-based Water-dispersible Assemblies with Enhanced Optoacoustic Performance for Multispectral Optoacoustic Imaging. *Nat. Commun.* **2023**, *14*, 3918.
(17) Yan, H.; Yin, X.; Wang, D.; Han, T.; Tang, B. Z. Synergistically Boosting the Circularly Polarized Luminescence of Functionalized Pillar[5]arenes by Polymerization and Aggregation. *Adv. Sci.* **2023**, *10*, 2305149.
(18) Zhao, X.; Zhou, X.; Cheng, Q.; Liu, Y. Blue Phosphorescent Solid Supramolecular Assemblies Between Hydroxypropyl-β-cyclodextrin and Triazine Derivatives for Achieving Multicolor Delayed Fluorescence. *Nano Today* **2025**, *60*, 102561.
(19) Qi, Z.; Wang, Q.; Qu, D.-H. Color-tunable Supramolecular Luminescent Materials for Information Anticounterfeiting. *Sci. China Mater.* **2025**, *68*, 962−978.
(20) Wang, X.; Ji, J.; Liu, Z.; Cai, Y.; Tang, J.; Shi, Y.; Yang, C.; Yuan, L. Chiroptical Sensing of Amino Acid Derivatives by Host−Guest Complexation with Cyclo[6]aramide. *Molecules* **2021**, *26*, 4064.
(21) Zhang, W.; Liu, M.-Q.; Luo, Y. Chiral Amplification and Regulation: Design and Applications of Circularly Polarized Luminescence-Active Materials Derived From Macrocyclic Compounds. *Aggregate* **2025**, *6*, No. e70039.
(22) Chen, W.; Li, B.; Gao, G.; Sun, T. Chiral Supramolecular Nanomaterials: From Chirality Transfer and Amplification to Regulation and Applications. *Interdiscip. Mater.* **2023**, *2*, 689−713.
(23) Liang, J.; Guo, P.; Qin, X.; Gao, X.; Ma, K.; Zhu, X.; Jin, X.; Xu, W.; Jiang, L.; Duan, P. Hierarchically Chiral Lattice Self-Assembly Induced Circularly Polarized Luminescence. *ACS Nano* **2020**, *14*, 3190−3198.
(24) Yang, X.; Jiang, W. Enantioselective Recognition of Functional Organic Molecules in Water by Biomimetic Macrocyclic Hosts. *J. Am. Chem. Soc.* **2024**, *146*, 3900−3909.
(25) Xu, Y.; Hao, A.; Xing, P. Structural Basis of Cucurbituril-containing Self-assembled Supramolecular Chiral Materials. *Angew. Chem., Int. Ed.* **2024**, *63*, No. e202409624.
(26) Jiang, H.; Zhang, L.; Chen, J.; Liu, M. Hierarchical Self-Assembly of a Porphyrin into Chiral Macroscopic Flowers with Superhydrophobic and Enantioselective Property. *ACS Nano* **2017**, *11*, 12453−12460.
(27) Zhu, H.; Li, Q.; Gao, Z.; Wang, H.; Shi, B.; Wu, Y.; Shangguan, L.; Hong, X.; Wang, F.; Huang, F. Pillararene Host-guest Complexation Induced Chirality Amplification: A New Way to Detect Cryptochiral Compounds. *Angew. Chem., Int. Ed.* **2020**, *59*, 10868−10872.
(28) Jiang, Z.; Chen, Z.; Yu, X.; Lu, S.; Xu, W.; Yu, B.; Stern, C. L.; Li, S.; Zhao, Y.; Liu, X.; Han, Y.; Chen, S.; Cai, k.; Shen, D.; Ma, K.; Li, X.; Chen, A. X.-Y. Engineering Helical Chirality in Metal-coordinated Cyclodextrin Nanochannels. *J. Am. Chem. Soc.* **2025**, *147*, 7325−7335.
(29) Inouye, M.; Hayashi, K.; Yonenaga, Y.; Itou, T.; Fujimoto, K.; Uchida, T.-a.; Iwamura, M.; Nozaki, K. A. Doubly Alkynylpyrene-Threaded [4]Rotaxane That Exhibits Strong Circularly Polarized Luminescence from the Spatially Restricted Excimer. *Angew. Chem., Int. Ed.* **2014**, *53*, 14392−14396.
(30) Yang, C.; Chen, W.; Zhu, X.; Song, X.; Liu, M. Self-Assembly and Circularly Polarized Luminescence from Achiral Pyrene-Adamantane Conjugates by Selective Inclusion with Cyclodextrins. *J. Phys. Chem. Lett.* **2021**, *12*, 7491−7496.
(31) Kazem-Rostami, M.; Orte, A.; Ortuño, A. M.; David, A. H. G.; Roy, I.; Miguel, D.; Garci, A.; Cruz, C. M.; Stern, C. L.; Cuerva, J. M.; Stoddart, J. F. Helically Chiral Hybrid Cyclodextrin Metal−Organic Framework Exhibiting Circularly Polarized Luminescence. *J. Am. Chem. Soc.* **2022**, *144*, 9380−9389.
(32) Tu, C.; Wu, W.; Liang, W.; Zhang, D.; Xu, W.; Wan, S.; Lu, W.; Yang, C. Host−Guest Complexation-Induced Aggregation Based on Pyrene-Modified Cyclodextrins for Improved Electronic Circular Dichroism and Circularly Polarized Luminescence. *Angew. Chem., Int. Ed.* **2022**, *61*, No. e202203541.
(33) Xu, H.; Lu, H.; Zhang, Q.; Chen, M.; Shan, Y.; Xu, T.-Y.; Tong, F.; Qu, D.-H. Surfactant-induced Chirality Transfer, Amplification and Inversion in a Cucurbit[8]uril−viologen Host−guest Supramolecular System. *J. Mater. Chem. C* **2022**, *10*, 2763−2774.
(34) Liu, G.-X.; Tian, C.-M.; Fan, X.-H.; Xue, X.-P.; Feng, L.; Wang, C.-H.; Liu, Y. Photocontrolled Reversibly Chiral-Ordered Assembly Based on Cucurbituril. *JACS Au* **2023**, *3*, 2550−2556.
(35) Dai, X.-Y.; Song, Q.; Zhou, W.-L.; Liu, Y. Cucurbit[8]uril Confinement-Based Secondary Coassembly for High Efficiency Phosphorescence Energy Transfer Behavior. *JACS Au* **2024**, *4*, 216−227.
(36) Yan, C.; Li, Q.; Miao, X.; Zhao, Y.; Li, Y.; Wang, P.; Wang, K.; Duan, H.; Zhang, L.; Cao, L. Chiral Adaptive Induction of an Achiral Cucurbit[8]uril-based Supramolecular Organic Framework by Dipeptides in Water. *Angew. Chem., Int. Ed.* **2023**, *62*, No. e202308029.
(37) Liu, Z.-X.; Lin, W.-J.; Liu, Y. Macrocyclic Supramolecular Assemblies Based on Hyaluronic Acid and Their Biological Applications. *Acc. Chem. Res.* **2022**, *55*, 3417−3429.
(38) Wu, Y.-L.; Sun, L.-H.; Chen, X.-K.; Liu, J.-W.; Ouyang, J.; Zhang, X.-D.; Guo, Y.; Chen, Y.; Yuan, W.; Wang, D.; He, T.; Zeng, F.; Chen, H.; Wu, S.; et al. Cucurbit[8]uril-based Water-dispersible

https://doi.org/10.1021/jacsau.5c01631
JACS Au 2026, 6, 621−630

Assemblies with Enhanced Optoacoustic Performance for Multispectral Optoacoustic Imaging. *Nat. Commun.* **2023**, *14*, 3918.
(39) Lu, T.; Chen, F. Multiwfn: A multifunctional wavefunction analyzer. *J. Comput. Chem.* **2012**, *33*, 580−592.
(40) Martínez, L.; Andrade, R.; Birgin, E. G.; Martínez, J. M. PACKMOL: A Package for Building Initial Configurations for Molecular Dynamics Simulations. *J. Comput. Chem.* **2009**, *30*, 2157−2164.
(41) Becke, A. D. Density-functional Thermochemistry. III. The Role of Exact Exchange. *J. Chem. Phys.* **1993**, *98*, 5648−5652.
(42) Weigend, F.; Ahlrichs, R. Balanced Basis Sets of Split Valence, Triple Zeta Valence and Quadruple Zeta Valence Quality for H to Rn: Design and Assessment of Accuracy. *Phys. Chem. Chem. Phys.* **2005**, *7*, 3297−3305.
(43) Grimme, S.; Ehrlich, S.; Goerigk, L. Effect of the Damping Function in Dispersion Corrected Density Functional Theory. *J. Comput. Chem.* **2011**, *32*, 1456−1465.
(44) Yanai, T.; Tew, D. P.; Handy, N. C. A New Hybrid Exchange-correlation Functional Using the Coulomb-attenuating Method (CAM-B3LYP). *Chem. Phys. Lett.* **2004**, *393*, 51−57.
(45) Frisch, M. J.; et al. *Gaussian 16*. Rev C.01; Gaussian, Inc.: Wallingford, CT, 2016.
(46) Zhang, J.; Li, R.; Bei, Y.; Xu, X.; Kang, W. Design of a Large Stokes Shift Ratiometric Fluorescent Sensor with Hypochlorite Detection Towards the Potential Application as Invisible Security Ink. *Spectrochim. Acta, Part A* **2023**, *285*, 121859.
(47) Zhang, W.; Zhang, Y.; Li, S.; Cui, Y.; Yu, J.; Liu, Y. Tunable Nanosupramolecular Aggregates Mediated by Host-guest Complexation. *Angew.Chem. Int. Ed.* **2016**, *55*, 11452−11456.
(48) Cao, X.; Yi, H.; Li, L.; Zhang, S.; Pan, H.; Chen, J.; Xu, J. Using a Fluorescent 1-methyl-4-(2-pyren-1-yl-vinyl)pyridinium Iodide to Characterize Solvent Polarities. *J. Appl. Spectrosc.* **2018**, *84*, 939−947.

https://doi.org/10.1021/jacsau.5c01631
JACS Au 2026, 6, 621−630